Surface & Coatings Technology 254 (2014) 104–111

Contents lists available at ScienceDirect

Surface & Coatings Technology

journal homepage: www.elsevier.com/locate/surfcoat

Wear and corrosion resistance of niobium–chromium carbide coatings on AISI D2 produced through TRD

F.E. Castillejo [a,b,*], D.M. Marulanda [c], J.J. Olaya [b], J.E. Alfonso [d]

[a] Grupo Ciencia e Ingeniería de Materiales (CIM), Universidad Santo Tomás, Street 9th, 51-11 Bogotá, Colombia
[b] Department of Mechanical Engineering and Mechatronics, Universidad Nacional de Colombia, Street 45, 26-85 Bogotá, Colombia
[c] Research Group in Energy and Materials (REM), Faculty of Mechanical Engineering, Universidad Antonio Nariño, Street 22 South, 12 D 81 Bogotá, Colombia
[d] Ciencia de Materiales y Superficies, Physics Department, Universidad Nacional de Colombia, Street 45, 26-85 Bogotá, Colombia

ARTICLE INFO

Article history:
Received 2 September 2013
Accepted in revised form 20 May 2014
Available online 10 June 2014

Keywords:
Nb–Cr carbide
Electrochemical impedance
Wear
TRD

ABSTRACT

Niobium carbide, chromium carbide and niobium–chromium carbide coatings were deposited using the thermo-reactive diffusion (TRD) deposition technique on AISI D2 steel substrates, and their wear and corrosion resistance was studied. The morphology of the coatings was characterized through optical and scanning electron microscopy (SEM), and the crystalline structure was studied through X-ray diffraction (XRD). Chemical composition was evaluated via energy-dispersive X-ray spectroscopy (EDS) and X-ray photoelectron spectroscopy (XPS). The hardness of the coatings was measured through nanoindentation, and their wear was studied using the ball on disk test. The electrochemical behavior was assessed with potentiodynamic polarization and electrochemical impedance (EIS) tests. The XRD results show the formation of the NbC for the niobium carbide coating, $Cr_{23}C_6$ and Cr_7C_3 for the chromium carbide coating, and NbC, $Cr_{23}C_6$ and Cr_7C_3 for the niobium–chromium coating. Hardness value for the niobium–chromium carbide coating was 27.62 ± 2.56 GPa, which was higher in comparison to 21.66 ± 0.5 GPa for niobium carbide, 14.7 ± 1.1 GPa for chromium carbide and 6.70 ± 0.28 GPa for the uncoated steel. The wear resistance obtained was higher for the niobium–chromium carbide coating. However, its corrosion resistance was lower than the corrosion resistance for binary coatings.

1. Introduction

Machine components and parts subjected to aggressive environments and strong wear conditions need surfaces with a high hardness and good corrosion resistance. Improvement of these characteristics is often performed through surface treatments that produce transition metal carbide or nitride layers. The techniques used to produce these coatings on an industrial scale are, among others, physical vapor deposition (PVD) and chemical vapor deposition (CVD) [1,2], which have advantages and limitations. For instance, both techniques require expensive and complicated equipment that must be operated under high-vacuum conditions, and the CVD process is done at high temperatures (700–1200 °C) in order to obtain a high deposition rate of the coating material. The PVD process can be performed at lower temperatures, but due to the limited amount of diffusion during the treatment, the adhesion of the coatings can be weak in some cases [3].

Another option for the production of coatings is the thermo-reactive deposition process (TRD). This technique was patented by Toyota in Japan and it has been applied successfully for many years at industrial level for producing several types of layers on iron-based alloys [4,5]. Among the advantages of the TRD process appears to be its low cost, because the treatment is performed at atmospheric pressure and it does not require an expensive equipment. The process is performed at high temperatures, similar to those used in CVD, and good adhesion of the coatings can be obtained. Some of the coatings that have been produced using this technique are chromium carbide (Cr_xC_y) [6] and niobium carbide (NbC), which exhibit very interesting characteristics for use in wear applications, such as a high hardness [7], great toughness and a high Young's modulus, together with a high melting temperature (3873 °C), which make it a good candidate for applications in high-temperature environments [8]. There have been several research projects concerned with niobium carbide (NbC) and chromium carbide (Cr_xC_y) coatings produced using TRD [9–13]. In all of these studies, only a carbide forming element (CFE) was added to the borax bath to form NbC [14] or CrC coating [15] deposited on AISI D2 steel. These studies have been focused on the microstructure, growth kinetics and mechanical properties of the coatings. However, to the authors' knowledge, no studies have reported on the mechanical and electrochemical behaviors of niobium and chromium carbide coatings. In this sense, the aim of this paper was to produce niobium carbide coatings (NbC), chromium carbide coatings (CrC), and a combination of niobium and chromium carbides using a borax bath with two types of CFE's (Nb

* Corresponding author at: Grupo Ciencia e Ingeniería de Materiales (CIM), Universidad Santo Tomás, Street 9th, 51-11 Bogotá, Colombia. Tel.: +57 5878797.
E-mail address: fabiocastillejo@usantotomas.edu.co (F.E. Castillejo).

http://dx.doi.org/10.1016/j.surfcoat.2014.05.069

and Cr) on AISI D2 steel substrates. Microstructure, wear, hardness and electrochemical performance were studied, and the results were compared with those obtained for binary carbides and uncoated steel.

2. Experimental procedure

The substrates were disks of AISI D2 steel, 15 mm in diameter and 4 mm in thickness, whose surfaces were polished with 1200 grit sandpaper. All surfaces were subsequently cleaned with acetone and immersed in isopropyl alcohol in an ultrasonic bath. The chemical composition of the steel, as stated by the manufacturer, is 1.5 wt.% C, 11.5–12.5 wt.% Cr, 0.15–0.45 wt.% Mn, 0.8 wt.% Mo, and 0.8 wt.% V and Fe balance. The steels were supplied in annealed condition with a maximum hardness of 2.6 GPa.

The thermal cycle of the steel started with preheating at 650 °C for 0.5 h, followed by the TRD process. The carbides were obtained using salt baths composed of molten borax ($Na_2B_4O_7$), aluminum (Al), and ferro-niobium (Fe–Nb) or ferro-chromium (Fe–Cr), depending of the coating to be deposited, as shown in Table 1. All treatments were performed at 1020 °C for 4 h and atmospheric pressure in an electrical furnace described elsewhere [16]. The chemical composition used for the baths was selected according to that suggested in another paper [17,18]. Quenching was performed in oil at room temperature after the TRD process and finally the treated pieces were subjected to tempering at 250 °C for 2.5 h.

As the rate growth of the niobium carbide layer and chromium carbide layer is controlled by niobium and chromium diffusion rates respectively, and carbon diffusion rate from steel to the corresponding layer, coating growth occurs as a consequence of the CFE's perpendicular to the steel sample [14]. According to this, the layer thickness varies with time as a parabolic law as follows:

$$x^2 = K_0 e^{-\frac{Q}{RT}} t \tag{1}$$

where x is the layer thickness, K_0 a pre-exponential constant, Q is the activation energy, R is the gas constant, T is the process temperature in Kelvin and t is the treatment time. K_0 and Q are obtained from the curve fit. As a result, the thickness of the coatings is calculated as shown in Table 2.

An X'Pert PRO PANalytical diffractometer was utilized to obtain X-ray diffraction patterns in order to identify the crystallographic phases present in the coatings. The equipment worked with the following settings: θ–2θ varying from 10° to 120°, monochromatic Cu Kα radiation (λ = 1.5409 Å), 45 kV, 40 mA and a 0.02° step size. The thickness of each coating and the wear track were observed using a Philips scanning electron microscope (SEM) functioning at 40 kV, after attacking the samples with Vilella 3%. Ten measurements were performed on the cross-sectioned sample in order to obtain an average thickness value. Energy dispersive X-ray spectroscopy (EDS) measurements were performed on the surface sample after cleaning with acetone and isopropyl alcohol in an ultrasonic bath in order to eliminate contaminants that result from the salt bath.

The hardness of the coatings was determined in accordance with ISO standard 14577 using an NTH2 nanoindentor from CSM instruments outfitted with a Berkovich indenter tip. A linear load was used with an approximate speed of 2000 nm/min, loading rate of 60 mN/min, maximum load of 30 mN and loading dwell time of 15 s.

Table 1
Chemical composition of the baths used in this work.

Sample	$Na_2B_4O_7$ wt.%	Fe–Nb wt.%	Fe–Cr wt.%	Al wt.%
S1	81	16	–	3
S2	67	–	30	3
S3	77	8	15	3

Table 2
Kinetics of the carbide layers produced by TRD.

Sample	K_0 (KJ/mol)	Q (cm^2/s)	T (K)	t (h)	x (μm)
S1	113.24	4.75×10^{-6}	1293	4	13.44
S2	111.31	3.88×10^{-6}	1293	4	13.7
S3	116.42	4.3×10^{-6}	1293	4	13.93

The chemical bonding state of the coating was determined through X-ray photoelectron spectroscopy (XPS). XPS spectra were recorded in an SPECS spectrometer in the constant pass energy mode at 50 eV, using Mg Kα radiation as the excitation source. Sample cleaning was performed using ion bombardment with Ar+ of 3.5 keV for 5 min in a preparation chamber (base pressure 2×10^{-7} mbar) connected through a gate valve to the main chamber. The calibration of the binding energy (BE) scale was checked using the C 1s signal (284.1 eV). X-ray spectroscopy (EDS) was done at a voltage of 20 kV and collection time of 120 s in a FEI Quanta 200 scanning electron microscope.

The tribological properties of the coatings were measured on a CETR-UMC-2 ball on disk tribometer using Al_2O_3 ball (6 mm diameter) as a sliding counterpart in air at room temperature. The sliding speed was selected as 50 mm/s and the load was fixed at 4 N. At the beginning of the test, the maximum Hertzian contact pressure, P_0, was 1.49 Pa and the radius of the contact circle, a, was 1.5×10^{-3} m, assuming a Young's modulus, E, of 380 GPa and a Poisson's ratio, ν, of 0.23 for Al_2O_3, as well as $E = 365.4$ GPa and $\nu = 0.23$ for the CrNbC coating, obtained using the nanoindentation test. The contact pressure and contact radius were used to determine the shear stress distribution along x, y and z directions for the two surfaces in contact, using the following expressions [19].

$$\sigma_x = \sigma_y = -P_0(1+\nu)\left\{1-\left[\frac{z}{a}\right]\tan^{-1}\left[\frac{a}{z}\right]\right\} + \frac{1}{2}\left[1+\frac{z^2}{a^2}\right]^{-1} \tag{2}$$

$$\sigma_z = -P_0\left[1+\frac{z^2}{a^2}\right]^{-1} \tag{3}$$

$$\tau_{max} = \left|\frac{\sigma_x - \sigma_z}{2}\right| \tag{4}$$

where σ_x, σ_y and σ_z are the shear stress along x, y and z directions, respectively, z is the depth of shear stress and τ_{max} is the maximum shear stress.

Fig. 1 shows the maximum shear stress and its distribution obtained using the Hertzian contact theory of mating pairs. The maximum shear stress is 165 MPa, located at a depth of ~1 μm below the coating surface.

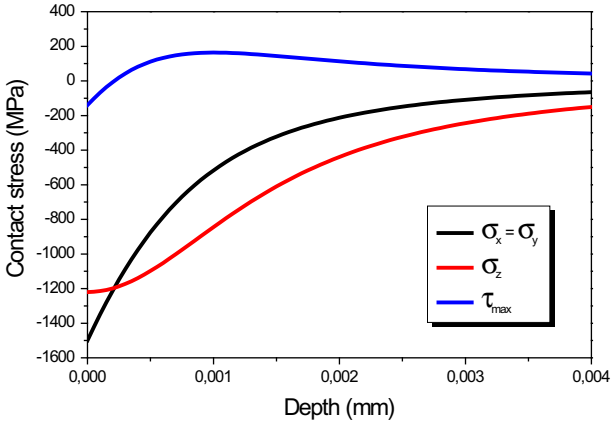

Fig. 1. Shear stress distribution in the niobium–chromium carbide coating on AISI D2 produced through TRD.

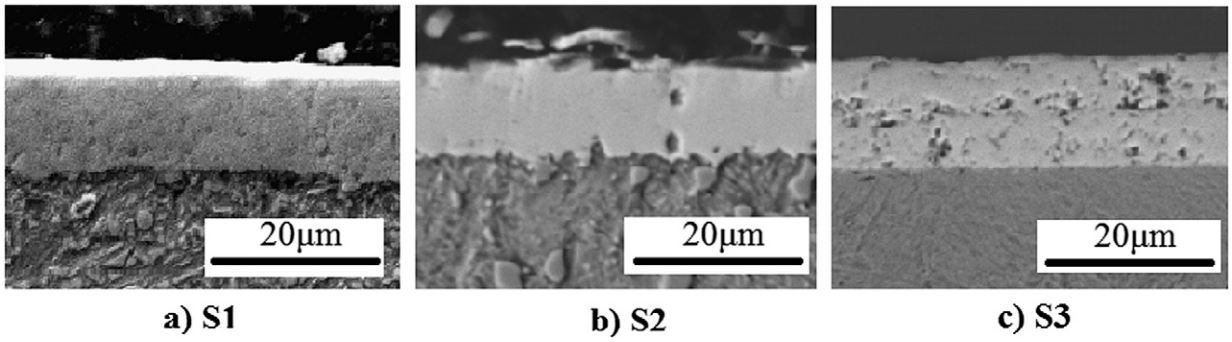

Fig. 2. SEM micrographs of the coatings produced on AISI D2 steel. a) S1, b) S2 and c) S3.

Finally, the corrosion resistance of the coatings was studied through potentiodynamic polarization curves and electrochemical impedance curves (EIS) using a Gamry Reference 600 Potentiostat/Galvanostat. The polarization measurements were performed using the ASTM G5 standard reference (ASTM G5, 1999). A saturated calomel electrode and high-purity platinum were used as reference (RE) and counter electrodes, respectively. The sample was used as a working electrode (WE) with a 0.196 cm^2 exposed area. After 1 h of immersion in 0.3% NaCl electrolyte, scans were conducted within the −0.5 to 0.6 V range, using a rate of 0.5 mV/s. Data were obtained using Echem analyst software. EIS tests were performed by varying the frequency from 100 kHz to 0.01 MHz, applying a sinusoidal voltage of 10 mV.

3. Results and discussion

3.1. Microstructure and thickness of the coatings

Fig. 2 shows SEM micrographs of the cross-section of the three samples (S1, S2 and S3) treated in the baths (Table 1). Homogeneous coatings with 15.7 ± 0.4 μm (S1), 13.1 ± 0.2 μm (S2) and 14.8 ± 0.1 μm (S3) thicknesses were obtained, and a clear interface between the coating and the substrate can be observed for all cases. These values are in agreement with the thickness calculated through Eq. (1) (see Table 2). Since the substrate is the same for all cases, the lower thickness obtained for S2 could be explained by the higher energy of formation of Cr_xC_y compared to NbC, which was measured in other works as −18 kcal [20] and −33.6 kcal [21] respectively. From the thermodynamic point of view NbC will grow easily than chromium carbide.

Fig. 3 shows the XRD patterns for the coatings obtained. For sample S1, niobium carbide was obtained NbC (JCPDS 00-038-1364) and for sample S2, a mixture of two phases of chromium carbide is observed: Cr_7C_3 (JCPDS 00-036-1482) and $Cr_{23}C_6$ (JCPDS 00-035-0783). The formation of two phases could be explained by the availability of carbon atoms in the process: at the beginning, the carbon atoms are distributed uniformly in the bulk substrate and the $Cr_{23}C_6$ phase is formed, according to the phase diagram, which can be found elsewhere [22]. As the diffusion process proceeds, the amount of carbon atoms increases on the surface and the Cr_7C_3 phase is formed. For sample S3, the three phases are shown.

Table 3 shows the results of EDS analysis of the coatings. It can be seen that the phase formation also depends on carbon atomic percentage.

As expected, there is a higher amount of niobium atoms in sample S3, due to the lower energy of formation for niobium carbide. On the other hand, no ternary carbides are observed, which could be explained by the hypothetical solubility of niobium in chromium. According to theoretical calculus, the enthalpies of formation for niobium carbide are very positive, which means almost zero solubility of niobium in chromium carbides [23,24]. According with the theoretical results reported in literature [23,24], the formation of ternary carbide between niobium and chromium is not probable at the pressure and temperature conditions used in this experimental work.

XPS analysis was performed on sample S3 in order to study the chemical bonding state of the coatings deposited. The results are shown in Fig. 4a–e. The typical overview is shown in Fig. 3a, and the detailed spectra of the Nb 3d, O 1s, C 1s and Cr 2p are shown in Fig. 4b, c, d, and e respectively. A high peak of oxygen is observed in Fig. 4a, which would indicate the formation of oxides in the film, because the spectrum was taken after etching for 5 min to eliminate surface oxygen. The high resolution XPS spectra the Nb 3d (Fig. 4b) shows three different spin–orbit doublets: the most intense one is characterized by a binding energy (BE) of the Nb $3d_{5/2}$ core level of 203.25 eV which is a characteristic of NbC [25]; the second component appears at a binding energy of the Nb $3d_{5/2}$ core level of 204.9 eV and can be associated to NbO_2 while the third component (BE of the Nb $3d_{5/2}$ core level, 207.1 eV) corresponds to Nb_2O_5 [26]. The result for NbC is in agreement with results reported for Nb–C in nanocomposites of Cu–NbC (203.7 eV)

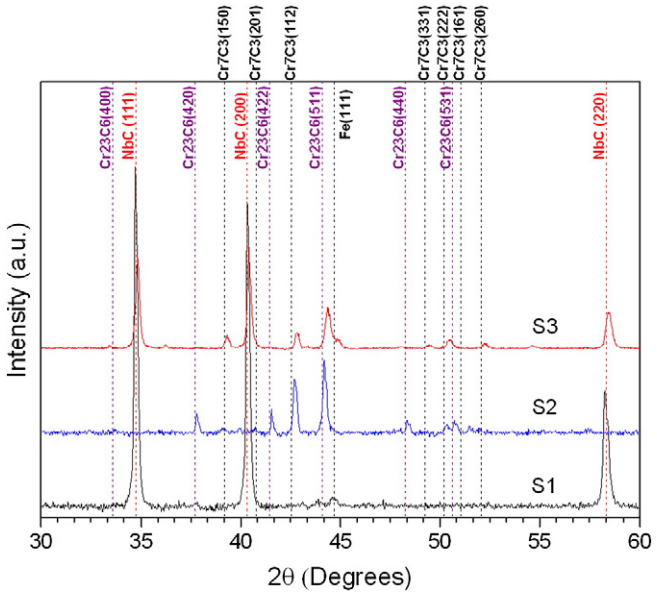

Fig. 3. XRD patterns of the carbide coating produced on AISI D2.

Table 3
EDS results for samples S1, S2 and S3.

Atomic %						
Sample	Nb	C	O	Cr	Fe	V
S1	27.19	48.99	23.82	–	–	–
S2	–	19.47	37.18	29.44	13.68	0.4
S3	19.01	42.4	25	4.62	8.98	0.55

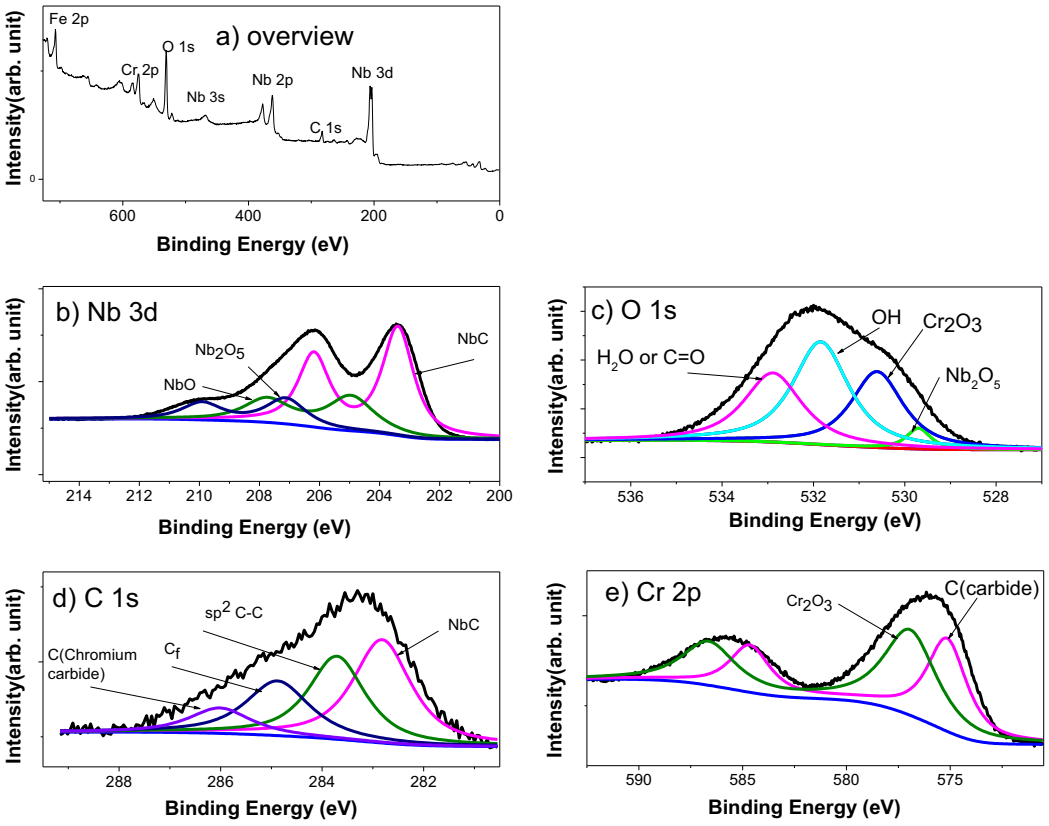

Fig. 4. XPS spectra for sample S3. a) Overview, b) Nb 3d, c) O 1s, d) C 1s spectra and e) Cr 2p spectra.

[25] and NbC coatings produced through magnetron D.C. (203.4 eV) [26]. Niobium oxide (NbO_2) may have been formed during the coating deposition at intermediate temperatures and niobium pentoxide (Nb_2O_5) could have been formed by the oxidation of NbC at high temperatures also during the TRD treatment for coating production. Niobium pentoxide has been found by other authors at similar BE of 207.66 eV [27] and 207.1 eV [26]. It was proposed that NbC on grain boundaries decompose to Nb and CO upon oxidation, allowing elemental Nb to diffuse over the grain boundary surfaces. This niobium oxidized to form niobium oxide Nb_2O_5 [28].

The peak O 1s (Fig. 4c) shows four contributions; i) 529.8 eV assigned to niobium oxide Nb_2O_5 [26], ii) 530.5 eV assigned to chromium oxide Cr_2O_3 [29], iii) 531.6 eV assigned to chromium hydroxide $Cr(OH)_3$, and iv) 532.9 eV associated with adsorbed water or C═O bonds. The formation of $Cr(OH)_3$ may be due to the oxidation of chromium at low temperature in a humid environment, and it has been reported in different positions (530.8 ± 0.4 [30], 531.3 [31]). The formation of Cr_2O_3 occurs at temperatures higher than 650 °C, mainly because of oxygen diffusion through grain boundaries and chromium diffusion through the bulk [32] during the TRD treatment.

The peaks corresponding to C 1s are shown in Fig. 4d. The binding energy at 282.83 eV can be assigned to the Nb–C bonding, which is also in agreement with results reported for this bonding in nanocomposites of Cu–NbC at a binding energy of 282.8 eV [25]. Another peak appears in the deconvolution at 283.75 eV, which is attributed to sp^2 C–C bonding, according to results reported in literature for this bonding at 284.4 eV [33] and 284.1 eV [34]. The presence of this bonding would indicate that surplus carbon atoms exist in the carbide like graphite or amorphous carbon on the surface, which is confirmed by the signal of a third peak at 284.9 eV which is attributed to free carbon atoms, and is in agreement with results reported in literature at 284.7 eV [35]. A fourth peak at 286 eV is attributed to carbon atoms in carbides, and may be due to the photoelectrons ejected from the carbon in Cr_3C_2 at 286.1 eV [35].

Finally, the XPS spectrum of Cr 2p energy region (Fig. 4e) shows two contributions at BE of 575.2 eV and 577.05 eV, according to results reported for Cr $2p_{3/2}$ species of Cr_2O_3 and Cr_3C_{2-x} ($0 \leq x \leq 0.5$) respectively [35], and results that have been reported by other authors [36].

Table 4
Crystallite size (D) and microstrain calculated for the samples.

Sample	Crystallite size D (nm)	Microstrain (%)
S1	257	0.1075
S2	356	0.1395
S3	97	0.1535

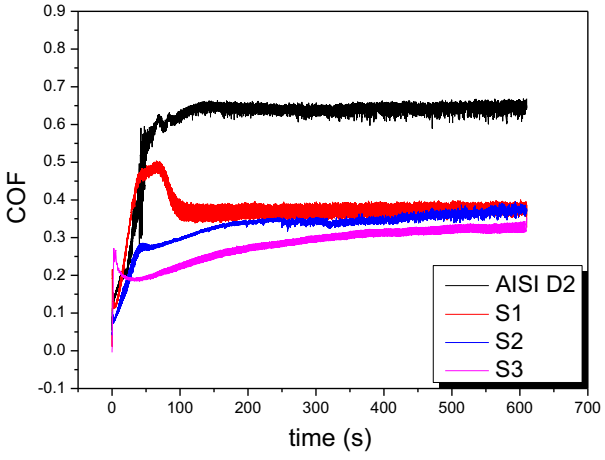

Fig. 5. Friction coefficient measurement of the coatings produced.

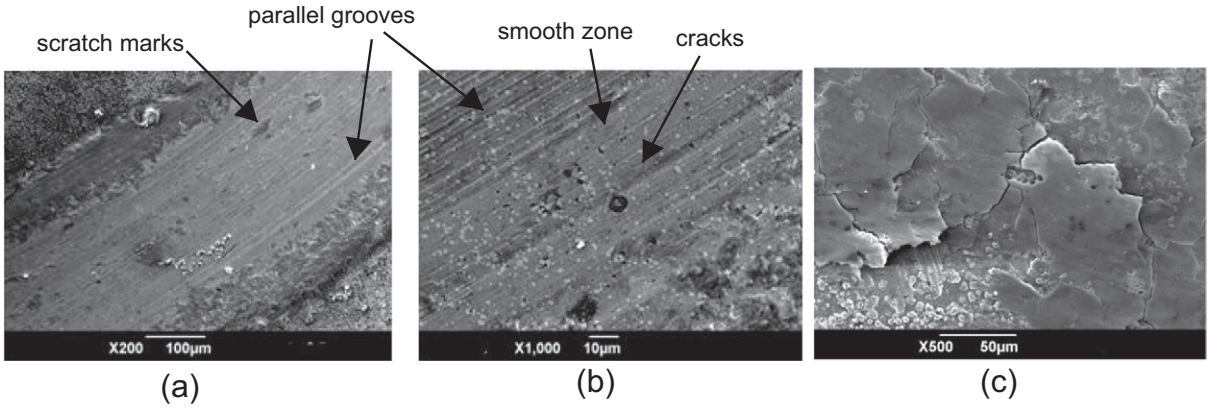

Fig. 6. SEM images of the ball on disk test. a) Optical micrograph of wear track. b) Detail of a specific zone of wear track.

The position for chromium carbide (575.2 eV) is shifted toward higher energies relative to pure chromium (574.1 eV [36,37]). This shift could be explained in terms of the particular bonding involved in the chromium carbides, where the bonding can be interpreted as a bonding with a metal, covalent and ionic percentage [38].

3.2. Hardness and tribological performance of the coatings

The hardness value measured for S3 was 27.62 ± 2.56 GPa. This value is higher than the hardness obtained for S1 (21.66 ± 0.5 GPa) and S2 (14.7 ± 1.1 GPa), which are in agreement with values reported for binary systems of niobium carbide (23.72 ± 0.93 GPa [39]) and chromium carbide (18.50 ± 0.35 GPa [40]) respectively. The hardness value obtained for S3 was also higher than the nominal value of steel AISI D2 after quenching (6.47 ± 0.41 GPa) which is in agreement with the results reported in other work [41]. This increase in hardness could be attributed to the presence of three different carbides in the coating with different crystal structures: face-centered cubic (NbC and $Cr_{23}C_6$) and orthorhombic (Cr_7C_3) and the incorporation of atoms with different sizes, which would cause large lattice distortions and a high solid-solution strengthening effect in the coatings [42]. In addition, hardness increase is also attributed to the formation of small crystallites in the coating. The crystallite size is associated with the widening of the diffraction peaks and was calculated using the Williamson–Hall (W–H) method [43]:

$$\beta = \frac{k\lambda}{D\cos\theta} + 4\varepsilon\frac{\sin\theta}{\cos\theta} + \beta_{inst} \quad (5)$$

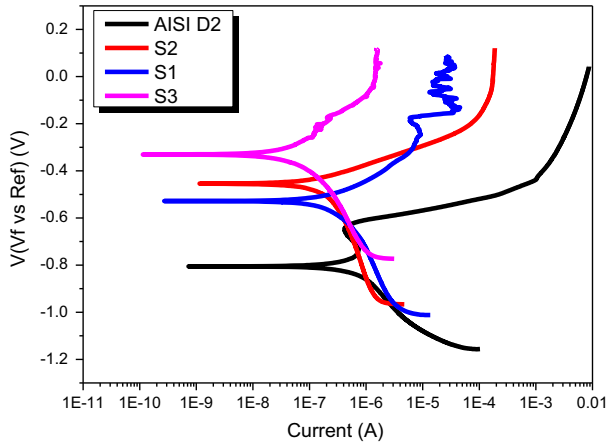

Fig. 7. Potentiodynamic curves for the uncoated AISI D2 steel and the NbC, $Cr_{23}C_6$ and Cr_7C_6 binary carbides and Nb–Cr carbide coating.

where β is the peak broadening, k is a non-dimensional constant which depends on crystallite geometry and was assumed as 0.94 for spherical crystals, λ is the radiation wavelength, θ is the Bragg's angle in radians, ε is the strain due to crystal distortion, β_{inst} is the instrumental broadening (measured as 0.035°), and D is the crystallite size. Strain (ε) and crystallite size (D) were obtained by fitting the curve $\beta\cos\theta$ vs. $4\sin\theta$, and they are shown in Table 4. It is clearly seen that crystallite size is smaller for S3, which also contributes to the increase in hardness.

Fig. 5 shows the graph of the friction coefficient (COF) against time obtained from the ball on disk (BOD) test performed on the coatings produced. A mean value of COF = 0.032 ± 0.014 was obtained for the niobium–chromium carbide coating. This value is lower than that for uncoated steel and could be associated with an excess of carbon atoms in the coating observed through XPS, which could be present in the form of graphite or amorphous carbon. The fact that secondary weak Van der Waals forces govern the bonding between the layers of graphite permits the layers to slide over one another, making it an ideal lubricant.

Fig. 6 shows SEM images at different magnifications of the wear track produced on the coating surface of sample S3. The presence of parallel grooves can be observed in Fig. 6a and b, and this wear mechanism is known as grooving wear or two-body abrasion [44]. This kind of wear is associated with the movement of abrasive particles (micro-cutting), which are produced from the contact between the two surfaces in the test and which are fixed to the ball surface during the process. The smooth zone indicates that rolling abrasion or three-body abrasion is exhibited by fine particles rolling through the contact zone. Some scratch marks are observed, which could be caused by debris activity, thus becoming embedded in the ball when the test is done [45]. Cracks are observed on the worn surface for the coating (Fig. 6c).

3.3. Tafel potentiodynamic polarization test

Fig. 7 shows the results for the potentiodynamic tests that were performed on the AISI D2 steel substrate and the three coatings produced, and Table 5 shows a summary of the values obtained.

From the results, it can be concluded that sample S3 exhibited greater corrosion resistance than both the uncoated steel and samples S1 and

Table 5
Tafel polarization parameters of bare and coated steels. Corrosion current (I_{corr}), corrosion potential (E_{corr}), anodic Tafel slope (β_a).

Sample	I_{corr} (A)	E_{corr} (V)	β_a (V/decade)
AISI D2	9.72E−07 ± 2.40E−08	805.5 ± 4.7	0.1543
S1	1.57E−07 ± 4.30E−08	529.4 ± 2.8	0.1048
S2	1.22E−07 ± 2.98E−08	458.6 ± 3.5	0.1796
S3	3.17E−08 ± 1.23E−09	329.4 ± 2.9	0.2025

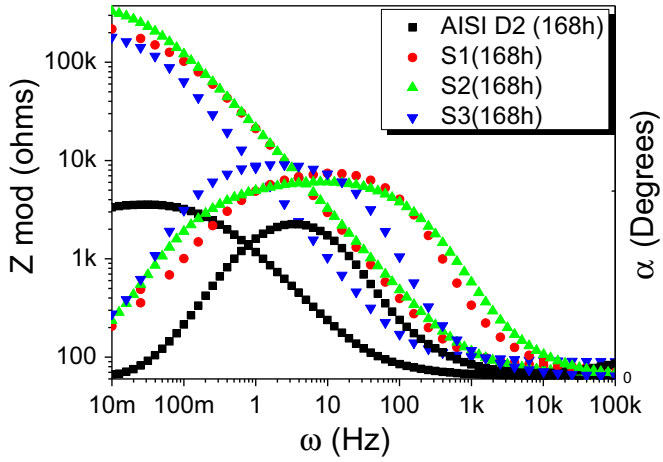

Fig. 8. Bode plots of EIS spectra of AISI D2 (uncoated), S1, S2 and S3.

S2, based on the lower current density (I_{corr}) and the higher value of corrosion potential (E_{corr}) observed for the Nb–Cr carbide coating (S3). This behavior can be explained by the presence of chromium oxide (Cr_2O_3) in the coating, which plays a key role in protecting steels because the inclusion of a highly stable chromium oxide can markedly decrease the corrosion rate through the passive film formed on the material's surface [46]. Furthermore, niobium oxide (Nb_2O_5) exhibits a high degree of chemical stability and good corrosion resistance [47].

3.4. Electrochemical impedance spectroscopy

Bode plots obtained from the EIS tests for an exposure time of 168 h in a 3% NaCl solution are shown in Fig. 8, for the AISI D2 steel substrate and the coatings produced. One time constant is observed for the uncoated steel, whereas two time constants are observed for the steel with different coatings, indicating the porous character of the coating, which allows the electrolyte to penetrate and reach the coating–substrate interface.

The equivalent circuits used to fit the plots are shown in Fig. 9. For the uncoated steel (Fig. 9a), a resistance R_{sol} is proposed, which is the resistance of the solution connected in series with two elements in parallel: a constant phase element for the substrate (CPE_s), where n is the exponent, and the polarization resistance (R_{pol}), which gives information about the corrosion resistance of the material. An n value of 1 indicates that the proposed element is completely capacitive, and if less than 1 it indicates that the element has both a capacitive and a resistive character [48].

For the coated steel (Fig. 9b), R_{sol} appears again, with CPE_c (constant phase element for the coating), whose exponent m behaves in the same way as n. The resistance to charge transfer across the pores in the coating, R_{por}, is included, along with the resistance to charge transfer across the coating–substrate interface, R_{cor}. Pore resistance plus charge transfer resistance is equivalent to R_{pol} in Fig. 9a ($R_{pol} = R_{por} + R_{cor}$).

The values of the parameters obtained after fitting of the equivalent circuits proposed are summarized in Tables 6a and 6b, for the steel AISI D2 and the coatings produced, after exposure times of 1, 24, 48, and 168 h. After 1 h, it can be seen that the impedance of the coatings is greater (Table 6b) compared to AISI D2 steel (Table 6a), which is in agreement with Tafel polarization results and could be explained by the presence of chromium and niobium oxides according to the XPS spectrums (Fig. 4). The impedance (R_{pol}) decreases with exposure time for all cases, which could be due to the increase in porosity with increasing time, which allows the electrolyte to penetrate and reach the coating–substrate interface. After 1 h of exposure, R_{pol} is greater for S3, which is in agreement with the results obtained in the Tafel potentiodynamic polarization tests (Fig. 7). After seven days of exposure, R_{pol} is minor for S3, indicating low corrosion resistance for this coating. This could be explained by the formation of stable oxides in the coating during its production as observed in the XPS spectra. After 1 h of exposure to the electrolyte, the formation of Cr_2O_3 and Nb_2O_5 may take place at a lower rate than in the thermal treatment. These oxides create a passive layer on the coating that protects the substrate from electrolyte penetration. However, after seven days of exposure, the electrolyte penetrates through pores and reaches the substrate, which decreases R_{pol} and therefore diminishes corrosion resistance. Better corrosion resistance is obtained for S2, which could be explained by the presence of $Cr_{23}C_6$ and Cr_7C_3 along with the formation of the stable oxide Cr_2O_3.

A quantitative measure of the porous character of a hard coating can be obtained using the electrochemical parameters measured experimentally via the following expression [48]:

$$P = \left(\frac{R_{p,s}}{R_{pol}}\right) \times 10^{\frac{|\Delta E_{corr}|}{\beta a}} \tag{6}$$

where P is the porosity, ΔE_{corr} is the difference between the corrosion potential of the steel and the coated steel, and β_a is the anodic slope. Both data points (ΔE_{corr} and β_a) were obtained from the potentiodynamic polarization testing (Table 5). $R_{p,s}$ is the polarization resistance of the uncoated steel and R_{pol} is the polarization resistance of the coated steel ($R_{pol} = R_{por} + R_{cor}$) [49]. The results are shown in Table 7. It is clear that the porosity increases slightly with exposure time, which indicates that it would take a long time for the electrolyte to penetrate the finer defects, such as microcracks.

The results in Table 7 show that the sample S3 exhibited a lower degree of porosity in comparison with S2 and S1, which could suggest that better electrochemical behavior is expected for this coating. However, crystallite size calculated for this sample is lower, which explains the good electrochemical behavior after 1 h of exposure, because long

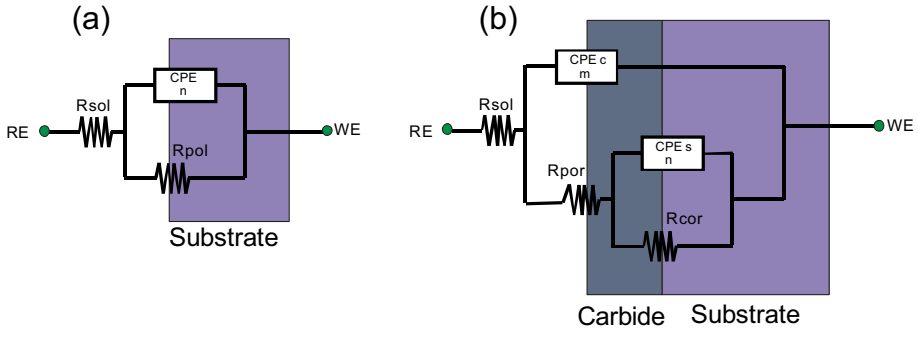

Fig. 9. Equivalent circuits: (a) Bare steel and (b) coated steels.

Table 6a
Electrochemical impedance parameters of the bare AISI D2 steel.

Sample	Exposure time	E_{corr} (mV)	R_{sol} (ohm)	R_{pol} (ohm)	(CPE_s)	n	Goodness of fit
AISI D2	1 h	−789	67	6481	1.21E−04	0.8	0.00116
	1 d		65	5290	1.14E−04	0.81	0.00135
	2 d		59	5175	7.46E−05	0.8	0.00231
	7 d		64	3698	1.75E−04	0.79	0.00168

Table 6b
Electrochemical impedance parameters for the coated steels.

Sample	Exposure time	E_{corr} (mV)	R_{sol} (ohm)	R_{pol} (ohm)	(CPE_s)	m	(CPE_c)	n	Goodness of fit
S1	1 h	−497	74.79	359,400	8.30E−06	0.74	9.03E−06	0.81	0.000252
	1 d		79.8	248,530	8.56E−05	0.91	9.91E−06	0.88	0.000635
	2 d		75.11	249,110	8.88E−05	0.97	9.83E−06	0.89	0.000791
	7 d		81.61	215,800	2.53E−05	0.62	9.01E−06	0.88	0.000857
S2	1 h	−460	81.56	924,820	7.60E−06	0.85	4.38E−06	0.88	0.000372
	1 d		72.41	656,745	5.83E−07	0.86	1.19E−05	0.8	0.000547
	2 d		80.09	632,333	3.65E−06	0.72	7.92E−06	0.86	0.000194
	7 d		69.7	327,900	2.37E−07	0.95	1.00E−05	0.82	0.000459
S3	1 h	−306	109	1,984,430	2.81E−06	0.64	3.85E−06	0.87	0.000105
	1 d		96.1	984,520	8.45E−07	0.78	1.63E−05	0.85	0.000151
	2 d		102.1	980,430	1.05E−06	0.69	1.87E−05	0.89	0.000568
	7 d		94.06	182,600	2.51E−06	0.76	2.19E−05	0.91	0.000567

paths through grain boundaries are present in the coating, which delays electrolyte penetration. After seven days, the electrolyte has reached the substrate, and corrosion resistance decreases.

4. Conclusions

In this paper, niobium–chromium carbide coatings were produced using the TRD process at 1020 °C for 4 h, and they were compared with binary coatings of chromium carbide and niobium carbide. The Nb–Cr coating had a hardness value of 27.62 ± 2.56 GPa, which was greater than the values obtained for binary coatings. This result is possibly due to the presence of two kinds of carbides in the coating with a different structure and a lower crystallite size in comparison with binary carbides. Wear resistance was also higher for the Nb–Cr coating.

The corrosion resistance of the chromium–niobium carbide (sample S3) was lower than the corrosion resistance for binary coatings. This was explained by the lower crystallite size and porosity of the coating. These results would indicate that the Nb–Cr coating could exhibit good performance in applications where good mechanical properties are required, but is not suitable for parts that are exposed to corrosive environments.

Table 7
Porosity of the different carbide coatings on AISI D2 steels.

Sample	ΔE_{corr} (mV)	Exposure time	P (%)
S1	292	1 h	0.0001227
	292	1 d	0.0003149
	292	2 d	0.0006582
	292	7 d	0.0009011
S2	329	1 h	0.0000244
	329	1 d	0.0000305
	329	2 d	0.0000316
	329	7 d	0.0000598
S3	483	1 h	1.25E−07
	483	1 d	4.33E−07
	483	2 d	8.45E−07
	483	7 d	9.37E−07

Conflict of interest

This work has no conflict of interest.

Acknowledgments

The authors gratefully acknowledge the financial support granted by the Departamento Administrativo de Ciencia, Tecnología e Innovación — COLCIENCIAS through project No. 338-2011, and the Fundación para la Promoción de la Investigación y la Tecnología (FPIT) through project number 2608. The authors acknowledge the support of the Universidad Nacional de Colombia (UNAL), Universidad Santo Tomás (USTA), and Universidad Antonio Nariño.

References

[1] J.L. He, Y.H. Lin, K.C. Chen, Wear 208 (1–2) (1997) 36–41.
[2] Y.L. Su, W.H. Kao, Wear 223 (1–2) (1998) 119–130.
[3] D.H. Kuo, K.W. Huang, Surf. Coat. Technol. 135 (2001) 150–157.
[4] B. Chicco, W.E. Borbidge, E. Summerville, Mat. Sci. Eng. A 266 (1999) 62–72.
[5] M. Aghaie-Khafri, F. Fazlalipour, J. Phys. Chem. Sol. 69 (2008) 2465–2470.
[6] Y.W. Chen, S.C. Fan, Mater. Chem. Phys 91 (2005) 192–199.
[7] T. Amriou, B. Bouhafs, H. Aourag, B. Khelifa, S. Bresson, C. Mathieu, Phys. B Condens. Matter 325 (2003) 46–56.
[8] B. Sustarsic, M. Jenko, M. Godec, L. Kosec, Vacuum 71 (2003) 77–82.
[9] A.R. Da Costa, A. Craievich, R. Vilar, Mater. Sci. Eng. A 336 (2002) 215–218.
[10] U. Sen, Thin Solid Films 483 (2005) 152–157.
[11] A. Bendavid, P.J. Martin, T.J. Kinder, E.W. Preston, Surf. Coat. Technol. 163 (164) (2003) 347–352.
[12] S. Duhalde, R. Colaco, F. Audebert, A. Perrone, A. Zocco, Appl. Phys. A 69 (1999) 569–571.
[13] S. Hotta, Y. Itou, K. Saruki, T. Arai, Surf. Coat. Technol. 73 (1995) 5–13.
[14] U. Sen, Mater. Chem. Phys. 86 (2004) 189–194.
[15] D.Y. Wang, K.W. Weng, C. Chang, W.Y. Ho, Surf. Coat. Technol. 120–121 (1999) 622–628.
[16] F. Castillejo, D. Marulanda, J.J. Olaya, O. Rodriguez, Dyna 170 (2011) 192–197.
[17] C.K.N. Oliveira, R.M. Muñoz Riofano, L.C. Casteletti, Mat. Lett. 59 (2005) 1719–1722.
[18] T. Arai, S. Harper, ASM Handbook, Heat Treatment, 4, ASM International, Materials Park, 1991, pp. 448–533.
[19] K.L. Johnson, Contact Mechanics, Cambridge University Press, UK, 1987. 1–468.
[20] T. Arai, N. Komatsu, M. Mizutani, J. Jpn. Inst. Met. 39 (1975) 247–255.
[21] W.L. Worrell, J. Chipman, J. Phys. Chem. 68 (April 1964) 860–866.
[22] M. Venkatraman, J.P. Neumann, Binary Alloy Phase Diagrams, ASM Handbook, 3, ASM International, Materials Park, 1990, p. 529.
[23] J.G. Costa Neto, S.G. Fries, H.L. Lukas, Calphad 17 (3) (1993) 219–228.
[24] A.V. Khvan, B. Hallstedt, K. Chang, Calphad 39 (2012) 54–61.

[25] M.T. Marques, A.M. Ferraria, J.B. Correia, A.M. Botelho do Rego, R. Vilar, Mater. Chem. Phys. 109 (2008) 174–180.
[26] M. Braic, V. Braic, M. Balaceanu, A. Vladescu, C.N. Zoita, I. Titorencu, V. Jinga, F. Miculescu, Thin Solid Films 519 (2011) 4064.
[27] C.F. Miller, G.W. Simmons, Robert P. Wei, Scr. Mater. 42 (2000) 227–232.
[28] J.E. Alfonso, J. Buitrago, J. Torres, J.F. Marco, B. Santos, J. Mater. Sci. 45 (2010) 5528–5533.
[29] Saıd Agouram, Franz Bodart, Guy Terwagne, J. Electron. Spectrosc. Relat. Phenom. 134 (2004) 173–181.
[30] A. Lippitz, Th. Hübert, Surf. Coat. Technol. 200 (2005) 250–256.
[31] L. Cunha, M. Andritschky, L. Rebouta, K. Pischow, Surf. Coat. Technol. 116–119 (1999) 1152–1160.
[32] T. Kacsich, K.P. Lieb, A. Schaper, O. Schulte, J. Phys. Condens. Matter 8 (1996) 10-703–10-719.
[33] Wu. Bo, Yu.Fu. Guoqiang Lin, Ming Hou, Baolian Yi, Int. J. Hydrogen Energy 35 (2010) 13255–13261.
[34] K. Zhang, M. Wen, Q.N. Meng, C.Q. Hu, X. Li, C. Liu, W.T. Zheng, Surf. Coat. Technol. 212 (2012) 185–191.
[35] Z. Zhao, H. Zheng, Y. Wang, S. Mao, J. Niu, Y. Chen, M. Shang, J. Refract. Met. Hard Mater. 29 (2011) 614–617.
[36] C.D. Wagner, W.M. Riggs, L.E. Davis, J.F. Moulder, G.E. Mullenberg (Eds.), Handbook of X-ray Photoelectron Spectroscopy, Perkin Elmer corporation. Physical electronic division, 1979.
[37] R. Teghil, A. Santagata, A. De Bonis, A. Galasso, P. Villani, Appl. Surf. Sci. 255 (2009) 7729–7733.
[38] M. Detroye, F. Reniers, C. Buess-Herman, J. Vereecken, Appl. Surf. Sci. 144–145 (1999) 78–82.
[39] C.K.N. Oliveira, R.M. Muñoz Riofano, L.C. Casteletti, Surf. Coat. Technol. 200 (2006) 5140–5144.
[40] S. Sen, Vacuum 79 (1–2) (2005) 63–70.
[41] C.K.N. Oliveira, C.L. Benassi, L.C. Casteletti, Surf. Coat. Technol. 201 (2006) 1880–1885.
[42] S.Y. Lin, S.Y. Chang, Y.C. Huang, F.S. Shieu, J.W. Yeh, Surf. Coat. Technol. 206 (2012) 5096–5102.
[43] G.K. Williamson, W. Hall, Acta Metall. 1 (1953) 22–31.
[44] K. Adachi, I.M. Hutchings, Wear 255 (2003) 23–29.
[45] K. Bose, R.J.K. Wood, Wear 258 (2005) 322.
[46] A.R. Trueman, D.P. Schweinsber, G.A. Hope, Corros. Sci. 40 (10) (1998) 1685–1696.
[47] S.H. Mujawar, A.I. Inamdar, C.A. Betty, V. Ganesan, P.S. Patil, Electrochim. Acta 52 (2007) 4899.
[48] C. Liu, Q. Bi, A. Leyland, A. Matthews, Corros. Sci. 45 (2003) 1243–1256.
[49] C. Liu, Q. Bi, A. Leyland, A. Matthews, Corros. Sci. 45 (2003) 1257–1273.